ANTIBACTERIAL PROPERTY OF COPPER OXIDE DECORATED REDUCED GRAPHENE OXIDE

Hridoy Saha

Roll:1611042

Md. Shafiq Aziz Himel

Roll:1611015

Bachelor of Science in Materials and Metallurgical Engineering

Bangladesh University of Engineering and Technology

Dhaka, Bangladesh

July 2021

COPYRIGHT STATEMENT

The following two notes on copyright and the ownership of intellectual property rights:

I. Copyright in text of this thesis rests with the author. Copies (by any process) either in full, or of extracts, may be made only in accordance with instructions given by the author. This page must form part of any such copies made. Further copies (by any process) of copies made in accordance with such instructions may not be made without the permission (in writing) of the author.

II. The ownership of any intellectual property rights which may be described in this thesis is vested in the department of Materials and Metallurgical Engineering of Bangladesh University of Engineering and Technology, subject to any prior agreement to the contrary, and may not be made available for use by third parties without the written permission of the department, which will prescribe the terms and conditions of any such agreement.

Approved page

The thesis titled "Antibacterial activity of copper oxide decorated Reduced graphene oxide" submitted by Hridoy Saha and Md. Shafiq Aziz Himel has been accepted for satisfactory submission in partial fulfilment of the requirements for the degree of Bachelor of Science in Materials and Metallurgical Engineering.

…….

Dr. Md Moniruzzaman

Department of MME BUET,

Dhaka

Candidate's Declaration

It is hereby declared that

1. The thesis submitted is my/our original work during under graduation at Bangladesh University of Engineering and Technology.
2. The thesis doesn't contain material previously published or written by others, except where this is appropriately cited through full and accurate referencing.
3. We have acknowledged everyone's contribution to the production of this thesis.

……

Hridoy Saha

Student ID: 1611042

Department of MME

BUET, Dhaka-1000

…….

Md. Shafiq Aziz Himel

Student ID:1611015

Acknowledgements

The authors would like to thank Dr. Md Moniruzzaman for his continuous supervision throughout the project. Without his invaluable advice and constant moral support, this project would have lacked direction and could not have been completed in due time. The authors would also like to thank all the honorable teachers of Department of Materials and Metallurgical Engineering for their valuable lessons and guidance during the four-year B.Sc. program. The authors are grateful to all the lab in-charges of Department of MME, BUET. Without their help, this work would not be finished in time. Lastly, the authors are thankful to almighty Allah to be able to successfully carry out this thesis work.

Abstract

Pathogenic bacteria are now quite resistant to traditional and frequently used biocidal treatment procedures. This fact is now becoming a major concern in a variety of settings, including water treatment, marine use and the medical industry. As a result, improved antibacterial technologies are required to prevent bacteria to form that are resistant to present and frequently used medicines. Copper oxide nanoparticles (CuONPs) decorated on reduced graphene oxide (rGO) are described as a potential pathogenic bacterial treatment in this work. Graphene-family nanomaterials offer fascinating properties and are used in a variety of applications, including antimicrobial action, cancer therapy, pathogen bio-detection, medication transport, and so on. Graphene based antibacterial property is a new kind of materials are showing various property. In this article we try to find out the resistance that show against bacteria by copper oxide decorated on reduced graphene oxide. The basic strategy involved to produce graphene oxide first by modified Hummer's method and then convert them into CuO decorated RGO by a single reaction. The particles are characterized with the help of X-ray diffraction (XRD), Transmission electron microscopes (TEM), Fourier-transform infrared spectroscopy (FTIR) and Energy Dispersive X-ray spectroscopy (EDS). XRD result indicate partially reduction of GO and monoclinic structure of CuO on rGO. It also indicates the normal particulate size of the prepared nanocomposite. TEM indicate if the copper oxide nanoparticles were widely distributed on rGO or not. The FTIR spectra revealed that oxygen functionality groups were added to GO, whereas they were severely reduced in rGO. EDS indicates the chemical analysis of the composite. Then measure their bacterial killing assay and measure inhibition zone and compare with normal graphene oxide. A thin film of bacteria put on a plate is treated to several antibiotics in the Disk Diffusion Antibiotic Sensitivity test (The Kirby-Bauer test). The Zone of Inhibition is a circular area surrounding the antibiotic's active site where bacteria colonies do not develop. Last of all we try to find out what is reason behind this particle which cause death of bacteria.

Contents

List of tables

List of Figures

CHAPTER 1: INTRODUCTION

1.1 Graphene History

Graphene originally made headlines in 2004 when two Manchester University academics, Sir Professor Andrei Geim and Sir Professor Kostya Novoselov, reported the finding of an electric field effect in an atomically thin two-dimensional material (2D) Graphene is a substance with only a few layers (FLG). [1] However, it became a widespread buzzword in popular culture. When this Manchester partnership was awarded the 2010 Nobel Prize in physics for their ground-breaking research on this extraordinary substance. A point worth noting here is that the scientists did not discover graphene, but rather made significant contributions to its isolation. mechanical exfoliation (repeated peeling) of graphite to produce a monolayer graphene sheet sufficient in size to appreciate its wondrous properties. However, graphene's history predates that.

Benjamin Brodie, a British chemist, saw Graphite Oxide for the first time in 1859 when he exposed graphite to strong acids. He didn't know what it was at the time.[2]The next important step in the history of graphene came when scientists used Transmission Electron Microscopy to look at it very closely (TEM).[3] In fact, one of these researchers came up with the name "Graphene." Hanns-Peter Boehm came up with the name.[47] There have been theoretical studies of Graphene going back to 1947, when Phil Wallace first calculated its band structure to figure out how bulk graphite works.[4] In 1995, Thomas Ebbesen and Hidefumi Hiura thought graphene-based nanoelectronics could be possible.[5]The surge in graphene research was made possible by several other well-known scientists, to whom we want to say thank you. Professor A. Geim [6]claims that the 'Graphene gold-rush' is because all previous graphene research was observational in nature. The limited electrical and optical studies listed above were performed on thin graphite films and were unable to assess the physics of graphene. The isolation of graphene crystals large enough to be subjected to thorough investigation to identify their electrical, mechanical, and optical properties was reported in a 2004 publication [1]. Their ‘scotch-tape' mechanical exfoliation process for graphene manufacturing was simple, effective, and inexpensive, allowing it to be quickly adopted by research groups all over the world. [48]

Graphene research is booming right now, thanks to its diverse set of features that make it useful for everything from solar cells to water filtration. To dispel the notion, new, inexpensive, and faster synthesis methods are being studied and reported. graphene qualities to the market as a result, graphene is attracting researchers from a wide range of natural science and engineering disciplines. Commercial graphene is still too costly for widespread use in research institutions around the world. As a result, graphene researchers use a variety of chemical and mechanical methods to extract graphene from graphite. The *Modified Hummer's* Method was used to produce graphene oxide (GO) from commercial graphite powder, which was subsequently reduced to produce rGO in this study. While rGO does not exhibit all of graphene's features, it is a viable low-cost alternative for the original material and excellent enough to imitate graphene's properties in laboratory experiments.

1.2 Properties of graphene

The atomic structure of graphene will aid in the exploration and explanation of its diverse properties.

A single sheet of carbon atoms densely packed into a benzene-ring structure is referred to as graphene. Each C atom is connected to its three neighbors with a bond and a -bond that are orientated out of plane in a 2D hexagonal configuration. It has sp2 hybridization, with the s, p_x, and p_y forming the bond and the remaining P_z forming the -bond. The -bonds combine to form half-filled bands, which allow electrons to flow freely and are responsible for most electronic characteristics. When exposed to C-containing compounds (such as hydrocarbons), holes in the structure have been found to self-repair, neatly aligning into hexagons. [49] Atomic waves on a 1 nm scale are found, which could be a result of the two-dimensional structure's instability.

Table 1 Properties and value of graphene

Properties	Value
Thermal conductivity, α	5.33103 $Wm^{-1}K^{-1}$
Resistivity, ρ	10^{-6} Ω-cm

Electron mobility, μ	1500 $cm^2 v^{-1} s^{-1}$
Transmittance	>95% for 2nm thick films >70% for 10 nm thick films
Coefficient of thermal expansion	$-6*10^{-4}$ /K
Specific surface area	2630 $m^2 g^{-1}$
Tensile strength, σ	130 GPa
Elastic modulus, E	0.5-1 TPa

1.2.1 Chemical properties

Due to the material's two-dimensional structure, all atoms are available for reaction from both sides. Defects in a sheet increase the chemical activity of the sheet. [7] Single layer graphene has been found to be more reactive than thick sheets [8] when oxidized below 2600°C [9]

1.2.2 Electrical properties

Graphene is a zero band-gap semiconductor. The electrons propagating through the honeycomb lattice behave like massless particles, so a 2D Dirac equation is used to describe them. Electron mobility is very high at room temperature but hampered by defects and contaminant molecules.

1.2.3 Mechanical properties

Graphene is the strongest material tested till now [10]with a tensile strength of 130 GPa and stiffness of 1TPa. It has lower system energy in wrinkled form, hence in the absence of lateral tension, the 2D structure will crumple into a fluctuating 3D form. This tendency explains the presence of wrinkles in pristine graphene sheets. Graphene has low fracture toughness, of about 4 MPa√m.[11] This indicates

that it is likely to undergo brittle fracture. It has also been observed that it has a greater ability to distribute force from impact, 10x more than steel per unit weight.

1.3 Applications of Graphene:

The inherent features of graphene have sparked a lot of curiosity in its potential application in a variety of technologies. Future generations of high-speed and radio-frequency logic devices, thermally and electrically conducting reinforced nanocomposites, ultra-thin carbon films, electronic circuits, sensors, and transparent and flexible electrodes for displays and solar cells are all examples of these [12]–[14]Graphene is currently available for purchase in the form of flakes, nanoparticles, and thin films.

CuO decorated Reduced graphene Oxide antibacterial property

Graphene is a 2D honeycomb-like lattice made up of a single, atomically thin sheet of carbon. Graphene's applications have been studied extensively since its separation. 0 including its potential use as a next-generation antimicrobial agent. As an active antibacterial agent, 2D graphene oxide has been widely used. Both in its native form and as a composite material. Most of the studies happened with silver nanoparticle which also show some amount of antibacterial property, but we can show other nanoparticle can also show some antibacterial property also. mounting evidence suggests that the antimicrobial activity may be primarily driven by the dissolution of copper ions, as well as the oxidative properties of copper.

1.4 Aim of the thesis

1. Synthesis of graphene Oxide
2. Produced Reduced graphene oxide from graphene oxide
3. Decorated with CuO oxide
4. Characterization of rGO and Reduced graphene oxide decorated with copper
5. By serial dilution method we compare the antibacterial property of RGO and CuO decorated RGO

CHAPTER 2: LITERATURE REVIEW

2.1Derivatives of graphene

2.1.1 Graphene Oxide

The cost effectiveness and easy scale-up potential of the methods used to generate graphene oxide make it appealing not only to produce graphene (by chemical exfoliation of graphite followed by a reduction process), but also as a material in and of itself. This is due to graphene oxide's ease of dispersion and potential as a composite ingredient. Graphene oxide composites outperform typical carbon composites in terms of thermal, electrical, and mechanical properties, even at extremely low loadings of the nanofiller component. As a result, learning about the structure and mechanical properties of graphene oxide is extremely important.

2.1.2Properties of graphene oxide

Lerf and Klinowski's widely regarded GO[21][22] model is a nonstoichiometric model (shown in Fig. 1). Hydroxyl and epoxy (1,2-ether) functional groups are used to adorn the carbon plane. Carbonyl groups can also be found in the sheet, most frequently as carboxylic acids near the sheet edge but also as organic carbonyl defects. The functional groups epoxy and alcohol are the most common. Apart from minuscule ripples [15], an ideal sheet of graphene contains solely trigonally connected sp^2 carbon atoms and is flat [16]. The densely decorated GO sheets are made up of sp^3 carbon atoms that are tetrahedrally linked and shifted slightly above or below the graphene plane [17]. GO sheets are atomically rough due to structural deformation and the presence of covalently linked functional groups [18]–[20]

Figure 1 Lerf-Klinowski model of GO

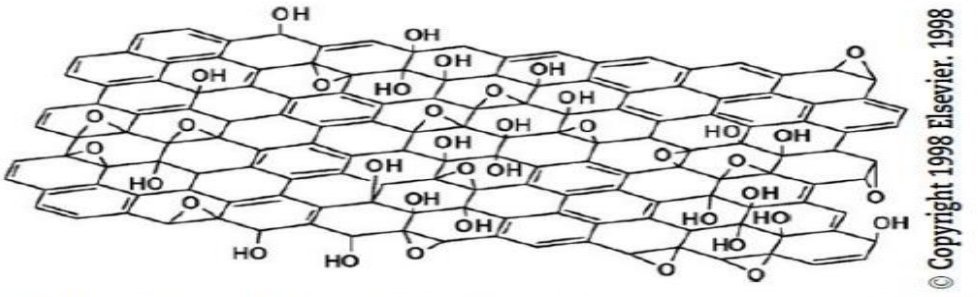

Fig 2.1: Lerf-Klinowski model of GO, excluding minor groups(carboxyl, carbonyl, ester etc.) on the surface.[45,46,47]

Graphite oxide's structure and properties are determined by the technique of synthesis and degree of ox idation. It usually has the parent graphite's layer structure, but the layers buckle and the interlayer spaci ng is about two times bigger (0.7 nm) than graphite's. GO's honeycomb lattice structure is mainly intact and remarkably comparable to Graphene, despite the significant presence of functional groups.[23]

As a result, GO can be defined as a random distribution of oxidized areas with oxygen-containing functional groups mixed in with non-oxidized regions where most carbon atoms maintain sp^2 hybridization. The hexagonal lattice's long-range conjugated network is responsible for graphene's conductivity. [24][25]By localizing the electrons, functionalization fractures, the conjugated network, limiting carrier mobility and concentration. Although GO has conjugated sections, it lacks continuous routes between the sp^2 layers, preventing classical transfer.

Scattering centers are formed by groups and defects, which impact the electrical characteristics of GO. Reducing GO restores some conductivity and brings the characteristics of graphene closer to those of pristine graphene.

With a thickness of 0.7 nm, the single layer graphene oxide membranes had an effective Young's modulus of roughly 156.5GPa (assuming zero bending stiffness) [50] and an elastic stiffness of around 109.6 N/m. In a nutshell, the Young's modulus of graphene is about a fifth of that of pristine graphene (1 TPa). For two- and three-layer membranes, the effective Young's modulus was around 223.9 GPa and 229.5 GPa, respectively. The close resemblance of the values for one, two, and three layers of graphene oxide is taken

to mean that the bonding between layers (two- and three-layer systems) is strong enough to prevent interlayer sliding

When exposed to water vapor or submerged in liquid water, graphite oxide is hydrophilic and rapidly hydrated, resulting in a significant increase in the inter-planar distance. Heating at 60–80 °C causes partial disintegration and degradation of the material, making complete removal of water from the structure appear impossible.

2.1.3Reduced Graphene Oxide (rGO):

Chemical reduction of graphene oxide is another method for synthesizing graphene.

However, the reduction process is inefficient, leaving residual oxygenated functional groups. Additionally, during the reduction process, lattice flaws are introduced. The experimental variation can be attributable to both experiment-specific and residual functional group-specific characteristics. 8 The reduction of GO is not only about removing the oxygen-containing groups bound to graphene and other atomic-scale lattice defects, but also about reconstructing the graphitic lattice's conjugated network. These structural alterations result in the reintroduction of graphene's electrical conductivity and other properties. Despite countless efforts, the goal remains a pipe dream. Because residual functional groups and defects significantly affect the structure of the carbon plane, it is inappropriate to refer to rGO as graphene, even today, because the characteristics are significantly different[16]

It was discovered that the conductivity of reduced graphene oxide scales inversely with the elastic modulus.[26]This, it is claimed, occurs because of oxygen bridges strengthening the sheet.[27]

Thus, a 24 percent increase in oxygen content results in a greater elastic modulus but a decrease in conductivity.

Unreduced sheets, on the other hand, with higher oxygen concentrations and conductivities many orders of magnitude lower did not exhibit an improved elastic modulus. This demonstrates that another factor influences the mechanical behavior. This is most likely owing to the existence of structural imperfections (holes or vacancies) that reduce the sheets' overall elasticity

2.1.4 E. coli bacteria

Escherichia coli belongs to the Enterobacteriaceae family, which includes gram-negative, facultatively anaerobic rod-shaped bacteria (with both fermentative and respiratory metabolisms) that lack the

enzyme oxidase. Escherichia coli cells are typically 1.1–1.5 millimeters wide, 2–6 millimeters long, and exist as single straight rods. They can be motile or nonmotile, producing lateral rather than polar flagella when motile. Along with flagella, many strains produce additional appendages such as fimbriae or pili, which are proteinaceous structures (or appendages or fibers) that extend outward from the bacterial surface and aid in adhesion to other cells or host tissues.

Escherichia coli's cell wall contains strain-specific O lipopolysaccharide antigens (at least 188 O antigens are currently recognized) and, if present, flagella, or H antigens (at least 53 H types are recognized). Additionally, there are numerous capsular polysaccharide (K) antigens. Serotypes of Escherichia coli are determined by the combination of O, H, and K antigens, although only the O and H types are typically listed, for example, E. coli O157:H7. Together with genome, virulence, and phage typing, serotyping of E. coli is a valuable epidemiological tool. Whole-genome sequencing is a technique that is increasingly being used to characterize E. coli and identify virulence genes. Nonpathogenic E. coli genome sequences are approximately 4.6 million bases in length, whereas pathogenic E. coli genome sequences are approximately 5.4 million bases in length. This genomic information enables us to better understand the relationships between different pathogenic groups of E. coli, the ability of isolates to cause disease, and the ability of isolates to transfer genetic material, potentially resulting in the emergence of new or more virulent types of E. coli.

Escherichia coli is closely related to Shigella spp., though Shigella is typically less biochemically active than most E. coli strains. Although Shigella and E. coli are genetically related, the two have historically been kept separate to avoid diagnostic confusion.[28]

2.2 Antibacterial Activity Assay

2.2.1 CFU Count

To conduct the experiment some equipments and materials were needed. Biological safety cabinet, autoclave, incubator, inoculation loop, petri dish, microwave oven, micro pippetes, test tubes were needed. Some chemicals were also needed such as, Isotonic saline solution, PBS (Phosphate buffered saline), Chromocult coliform agar, Eb broth to grow *Escherichia coli* ATCC 8739 bacteria and stock bacteria solution.

First, we need to do serial dilution. To do the dilution we have to make several 9ml solution of eb broth. We also must make the stock solution. We must select the suitable dilution factor to count CFU (colony forming unit). We select the dilution factor based on the number of colonies.

Serial dilution: A series of consecutive dilutions is used to lower a dense culture of cells to a more acceptable concentration. Each dilution lowers the bacterium concentration by a certain amount. It is feasible to determine how many germs you started with by calculating the overall dilution for the entire series.

Figure 2 Serial dilution

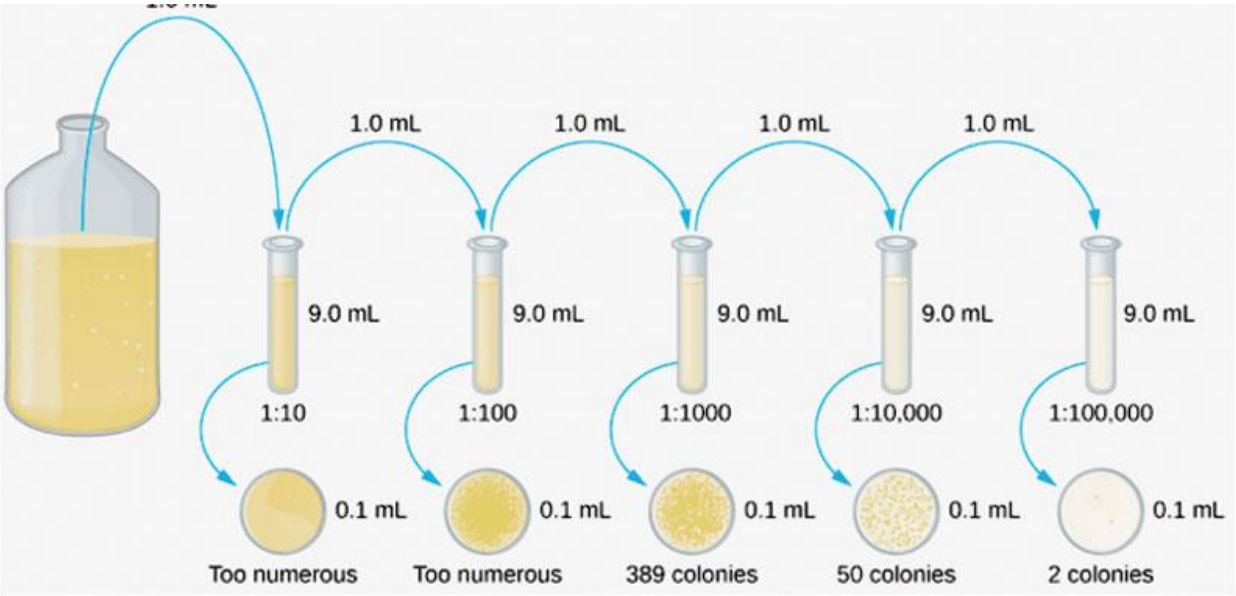

Chromocult coliform agar (2.65g) is to be taken in 100 ml distilled water in a beaker. Then it has to be boiled the media at 100°C for 1 minute. Then the media will be rotated to mix the content and heat will be applied. Then 15 ml of this solution is poured in sterile petri dish and allowed the solution to cool down and solidify. Thus, the agar media is prepared. With a sterile inoculation loop bacteria are taken from the serially diluted stock bacteria solution and struck them on the agar media like figure 9. Then the petri dished are incubated in an incubator at 37°C for 24 hours. In accordance with the Association for the Advancement of Medical Instrumentation recommendations all cultures should be incubated at 37 degrees C for 24 h on suitable culture media as 37°C is normal body temperature of humans so the pathogens grow greatly at this temperature. Thus, the control solution is made. To the inoculated broth, 2 mg/ml of synthesized GO, rGO/Cu(s), or rGO/Cu(rg) was added, and the samples were incubated at 37°C to make to measure the antibacterial assay of the solution.

As the positive controller (for 1 mg/mL), rGO (10 mg) was added to sterilized PBS (9 mL) solution, whereas another PBS (9 mL) solution was made at the same time but did not receive the rGO-CuONP hybrid as the negative controller. Autoclaved EB broth media was inoculated with E. coli bacteria colonies and cultured at 37 °C for 24 h until bacteria growth achieved an approximate E. coli concentration of 10^6–10^7 CFU/mL. As the positive controller (for 1 mg/mL), rGO (10 mg) was added to sterilized PBS (9 mL) solution, whereas another PBS (9 mL) solution was made at the same time but did not receive the rGO-CuONP hybrid as the negative controller. Each PBS was inoculated with 1 mL of E. coli and placed in a shaking incubator at 175 rpm for 3 h contact time. From the positive and negative controllers of E. coli cultures, a sterile PBS dilution solution series (9 mL each) was made, and 100 mL of a fourth diluent was plated on a freshly constructed sterile LB agar plate using a sterile spreader. The environmental controllers of EB−agar plates did not get E. coli culture from the diluents. Assays were carried out in duplicate. The plates were inverted and incubated for 24 hours at 37 degrees Celsius. In triplicate, the protocol was followed with 20 mg and 30 mg of rGO-CuONP for 2 and 3 mg/mL concentrations, respectively. For E. coli, the entire technique was followed in triplicate for control, rGO and rGO- CuONP materials. [29]

Figure 3 Settling bacteria on petri dish

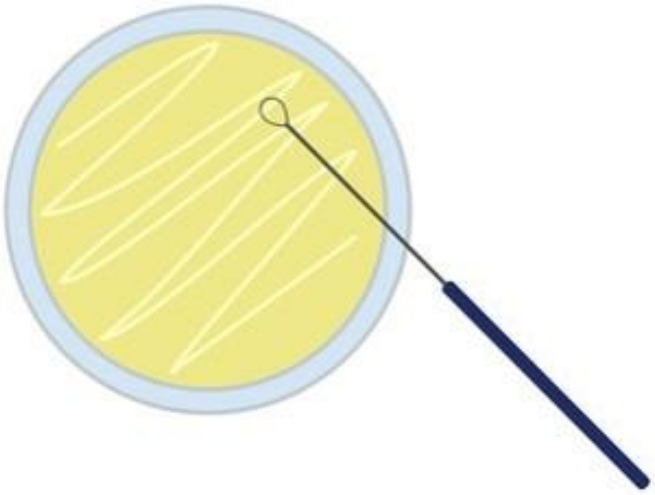

After incubation, we will see some purple dots along the strikes. The dots are the bacterial colonies. We can count the number of colonies. If the number is more than 300, we call it TNTC (too numerous to count) If it is less than 30, it is TFTC (too few to count). 30≤number of colonies≤300 is the sweet spot.

We select the dilution factor which satisfies the upper condition.

The colony forming units in a unit volume were manually computed to derive the mean and standard deviation from digital photographs of the plates.

$$\text{CFU/ml} = \frac{\text{no. of colonies} \times \text{dilution factor}}{\text{volume of culture plate}} \text{ [29]}$$

2.2.2 Inhibition Zone

A thin film of bacteria put on a plate is treated to several antibiotics in the Disk Diffusion Antibiotic Sensitivity test (The Kirby-Bauer test). The Zone of Inhibition is a circular area surrounding the antibiotic's active site where bacteria colonies do not develop. The zone of inhibition can be used to determine a bacteria's sensitivity to an antibiotic. [30]

Different dosages (20, 40, 60, 80, and 100 L) of GO and rGO-CuO nanocomposites aqueous dispersions were applied to a 10 mm filter paper, dried, and sterilized for 60 minutes using a UV lamp. On TSA, test bacterium lawns (1×10^6 CFU/plate) were created. The sterilized samples were then placed on the lawns with care, with empty filter paper serving as a control. The plates were incubated for 24 hours at 37 degrees Celsius. The diameter of the inhibition zone was then measured to determine the inhibitory activity of the investigated materials on bacteria growth. [31]

Figure 4 Inhibition Zone

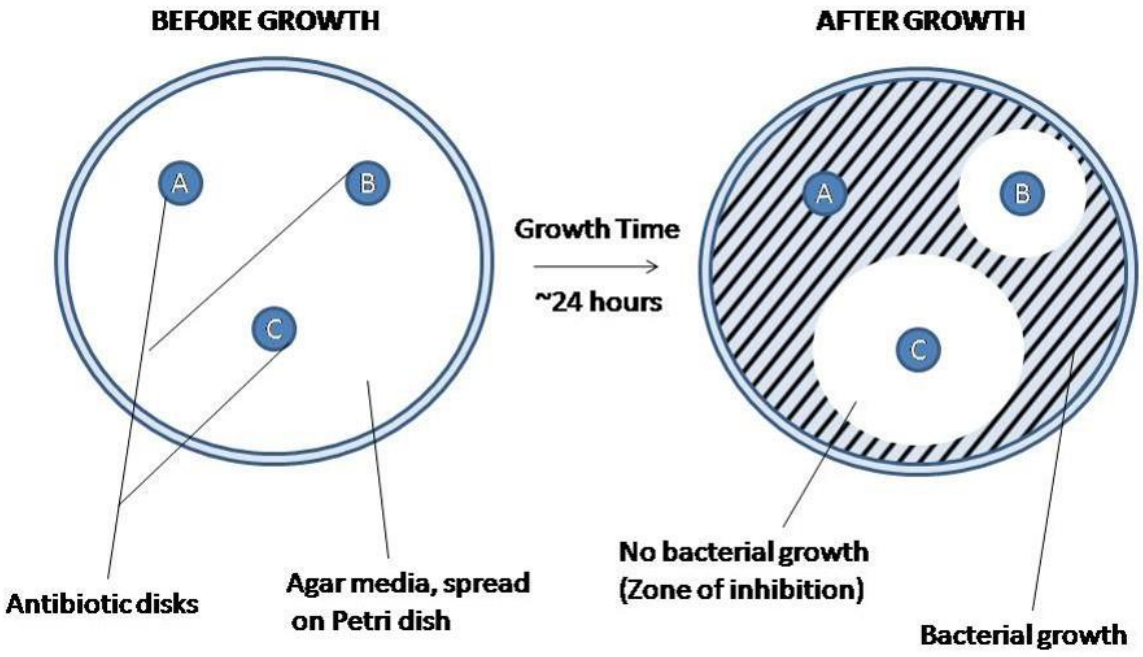

Measurement of diameter: Converting the image to grayscale is the initial stage in the Zone recognition process. Only the intensity is required to distinguish the zones, which are not distinguishable by luminance

or chrominance. As a result, a grayscale image is ideal. Other benefits of changing to grayscale include reduced image noise, reduced complexity, and faster processing. In the second frame of Figure 10, you can see a grayscale image of a computer-generated test image of a petri dish.

After converting the image to grayscale, the antibiotic-affected portion of the petri-dish must be isolated from the rest of the bacteria pool. The threshold value is used to distinguish these sections based on their intensity. [30]

Figure 5 A grayscale image can be created from the colorful test image. Using contour detection, the third image is created.

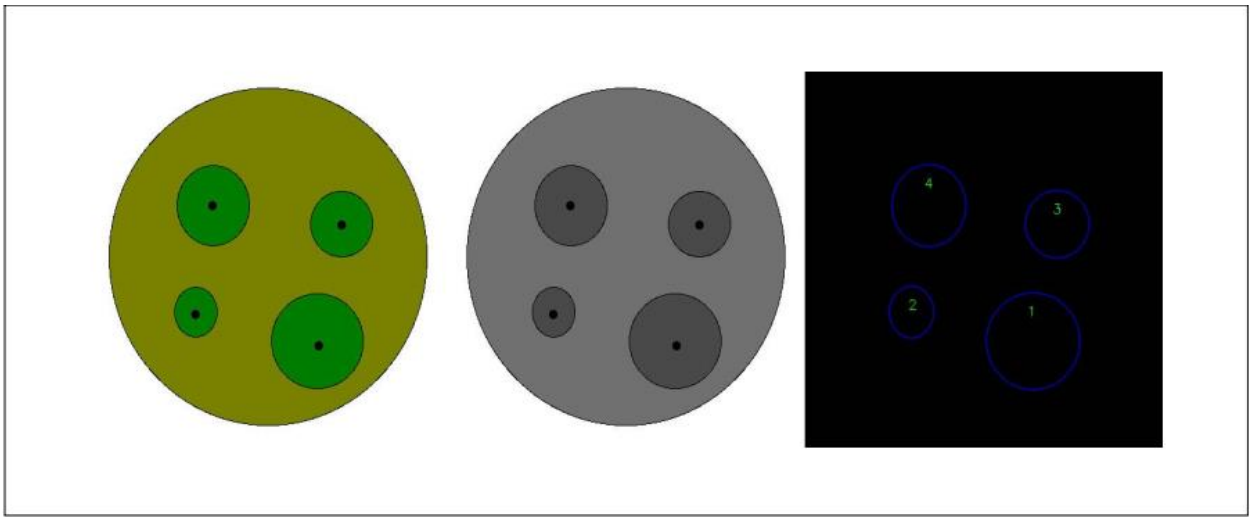

As a result of contour detection, each antibiotic now has an array of contour sequence points (the contours for the test image may be seen in the third frame of Figure 10). This array aids in the analysis and discovery of properties such as the detected region's area and centroid. Following that, the centroid of each contour must be established. This is accomplished by averaging the axes of the sequence points obtained. [30]

The area of each contour may be determined once the contours have been marked. Only contours whose area falls inside a particular range are considered. Small image distortions can thus be avoided in this manner. [30]

Using the equation below, which is a metric for determining bacterial sensitivity/resistance, the diameter of the Zone of Inhibition can be derived from the area measured in the previous step. [30]

$$\text{Diameter} = \sqrt{\frac{\pi \times \text{Area}}{4}}$$

The numbers obtained from the system, however, are in pixels rather in centimeter or millimeter gradients. As a result, additional step is required to convert pixels to centimeters or millimeters. [30]

CHAPTER 3: EXPERIMENTAL PROCEDURE

3.1 Synthesis of Graphene Oxide (GO):

To produce graphene oxide, the Modified Hummers' Approach was applied, which is slightly different from the traditional Hummers' Method. This method helps to produce grapheme oxide more easily and it is time effective. Besides, it removes the possibility of involvement of toxic gases which are not environment friendly.

3.1.1 Chemical materials

Graphite powder and Polyvinyl Alcohol (PVA) powder was purchased from Qualikems Fine Chem. Pvt. Ltd. Sulfuric Acid (H_2SO_4) (98%) and Hydrogen Peroxide (H_2O_2) (30%) were obtained from Merck (Darmstadt, Germany). Potassium permanganate ($KMnO_4$) was obtained from Merck, India. Sodium Nitrate ($NaNO_3$) was obtained from Guangdong Chemicals. Hydrazine Hydrate (80%) was used as reducing agent. The chemicals were used without further purifications. Deionized water (DI water) was used throughout the experiments.

3.2.2 Experimental Procedure:

- Graphite (12g) and $NaNO_3$ (6g) were mixed in 276 mL of H_2SO_4 (98%) in a volumetric flask (Graphite: NaNO3 = 2:1) It was kept under continuous stirring for 30 minutes (using magnetic stirrer) and cooled to 0oC by putting it in an ice bath.
- $KMnO_4$ (36g) was added to this mixture at a rate so that the temperature remained $<20^0$C. The solution was continuously stirred using a glass rod.
- Ice bath was removed, and temperature was raised to 35^oC. It was then stirred for 30 minutes until the mixture became pasty with brown-grey color. Then maintaining a temperature of 65^oC on a hot plate, it was heated for 1 hour.
- Deionized water (552 ml) was added slowly and carefully. The exothermic reaction will produce much heat. The temperature was kept to 98^oC for 15 minutes. The mixture became brown.

- The solution was diluted with water (530 ml). 60 ml H_2O_2 (30%) was added to this solution and stirred at 70°C for 2 hrs. The solution changed to coffee color. $H_2O_2$is added for complete removal of KMnO4. Water is used to stop oxidation reaction.
- The solution was filtered whilst still warm to form a solid cake and then washed three times with a total of 1680 ml of water.
- The solid cake was separated from the filter paper with blade.
- Then it was put into a falcon tube with De-Ionized (DI) water for centrifugation. Centrifugation was done at 8000 rpm for 15 minutes.
- Obtained precipitate was mixed with De-Ionized (DI) water. ¬ Then the mixture was ultrasonicated for 45 minutes to form homogeneous dispersion of solute and to remove additional impurities.
- Then it was dried at 70°C for 24 hours to get hard solid Graphene oxide (GO). Grinding was performed to obtain desired GO powder. Obtained powder was hydrophilic in nature.

Figure 6 Mixing all chemical reagent

Figure 7 stirring with magnetic stirrer 30 minutes

Figure 8 $KMnO_4$ powder

Figure 9 KMnO4 in ice bath

Figure 10 Mixing and heating

Figure 11 Mixing and measuring temperature

Figure 12 filtering

Figure 13 After filtration

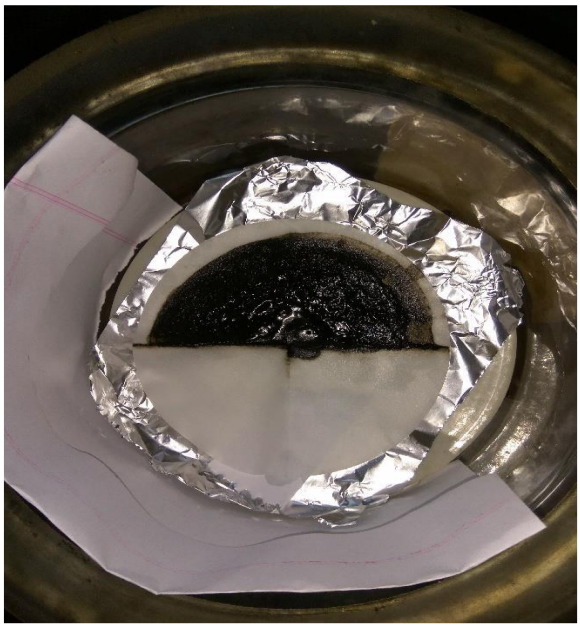

Figure 14 centrifugation machine

Figure 15 During centrifugation

Figure 16 Sample preparation

Figure 17 after centrifugation

Figure 18 Before ultra-sonication

Figure 19 Completed soication

Figure 20 sonicator

Figure 21 During experiment

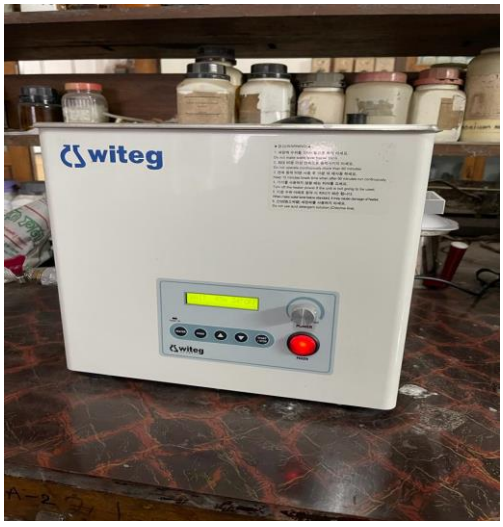

3.2 synthesis of CuO decorated reduced graphene oxide procedure

3.2.1Chemical and materials

PQ11, $Cu(OAc)2H_2O$, urea, and H_2O_2 (30%) were purchased from Aladin Ltd. (Shanghai, China). $NaNO_3$, RhB, H_2SO_4 (98%), and KMnO4 were purchased from Beijing Chemical Corp. All chemicals were used as received without further purification. The water used throughout all experiments was purified through a Millipore system.[32]

3.2.3 Synthesis of CuO decorated Reduced graphene oxide

- Kuon/rGO nanocomposites were prepared by heating the mixture of $Cu(OAc)_2.H_2O$ and GO in the presence of PQ11 and urea.
- 26 mg of $Cu(OAc)_2.H_2O$ and 16 mg of urea were added into 10 mL of ethanol.
- 1 mL of 0.67 M PQ11 was added and also 1 mL of GO (0.5 mg mL1) solution.
- Sonicated the solution for 20min
- The solution transferred into autoclave and heated there for about 40min at 180^0 C
- The solid products were obtained by centrifugation, washed by water and ethanol, and dispersed into water[32]

Figure 22 the formation of CuONF/rGO nanocomposites

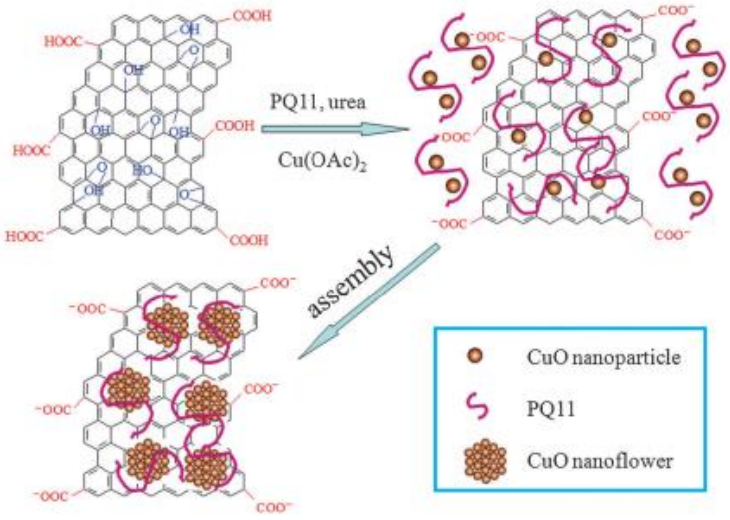

3.3Antibacterial activity of the nanocomposite flat surfaces

3.3.1 Chemical and materials

Luria-Bertani (LB) broth, phosphate-buffered saline (PBS; pH 7.5),

3.3.2 Experimental procedure

- The bacterial cells were grown overnight at 37 °C and 150 rpm in Luria-Bertani (LB) broth.
- After incubation, the bacterial cells were centrifuged at 8000 rpm in phosphate-buffered saline (PBS; pH 7.5) three times.
- Final bacterial cell concentration was adjusted to an optical density of 0.2 using a spectrophotometer at 600 nm.
- Bacterial cell viability was determined using the colony forming unit (CFU) counts. 1 cm × 1 cm of the nanocomposite film was placed in a 24 well plate.
- 50 µL of the bacterial cell suspension was exposed to the surface for 3 h at room temperature.[33]

3.4 Antibacterial mechanism

3.4.1. Glutathione oxidation assay

Acellular assessment of glutathione oxidation was conducted with little modification [24,44]. A 1 cm × 1 cm nanocomposite surface was placed in a 24 well plate and 0.8 mM glutathione dissolved in 50 mM bicarbonate buffer (pH 8.6). (pH 8.6). The samples were incubated at room temperature in the dark under 150 rpm shaking for 3 h. After incubation 0.05 M Tris-HCl and 15 µL of Ellman's reagent (5,5’-dithiobis (2-nitrobenzoic acid), were added into the mixture to yield a yellow product. A 200 µL sample of the solution was withdrawn and put in a 96 well plate. The unoxidized glutathione was quantified spectrophotometrically using a microplate reader at an absorbance of 412 nm.[33] Glutathione solution without contact with any material was used as a negative control while 1 mM hydrogen peroxide was used as a positive control. The loss of glutathione was calculated using Equation

$$\text{Loss of glutathione} = \frac{\text{Absorbance of negative control} - \text{Absorbance of sample}}{\text{Absorbance of negative control}} \times 100$$

3.4.2 Detection of reactive oxygen species (ROS)

The production of four crucial ROS (superoxide radical anion $O_2\%^{-}$, hydroxyl radical $^{\bullet}OH$, hydrogen peroxide H_2O_2 and singlet oxygen $^1O_2$) was monitored a cellularly using respective chemical probes. Details are described in the Supporting Information. [33]

CHAPTER 4: CHARACTERIZATION

4.1 XRD

The nature of the rGO on the electrode surface was also investigated using the XRD technique (Figure 23). The distinctive peak of the XRD pattern of GO was at 2θ = 10.5°, with an interlayer spacing of 0.84 nm (obtained using Bragg's Law equation: n = 2dsinθ). Due to the presence of oxygen containing groups in the nanosheets, this value is significantly higher than the 0.335 nm for graphite, indicating a considerable distance between the planes of GO sheets (Figure 23A). In comparison to GO, the height of the peak at around 10 was reduced in rGO (Figure 23B), and a new broad peak around 25 appeared, corresponding to the hexagonal structure of graphene. The decrease in peak height at around 10 could be attributable to a partial reduction of GO, which was consistent with electrochemical results. [34]

The CuO(NP)/rGO XRD pattern (Figure 23C) showed distinct peaks at 2θ = 32.2, 35.5, 39.1, 49.1, 54.1, 58.3, and 66.4, which were assigned to the monoclinic crystal structure of CuO nanoparticles reflection lines. The diffraction measurements obtained were in good agreement with the CuO JCPDS card (JCPDS80–1268). $Cu(OH)_2$ and Cu_2O peaks were not found, indicating that the CuO product in the nanocomposites was of high purity. Furthermore, no traditional graphene sheet stacking peak was found. These findings demonstrate that reduced GO nanosheets were spread among CuO nanoparticles, which is in line with previous findings. [34]

Figure 23 X-ray diffraction (XRD) image of (A) GO, (B) rGO and (C) CuO(NP)/rGO

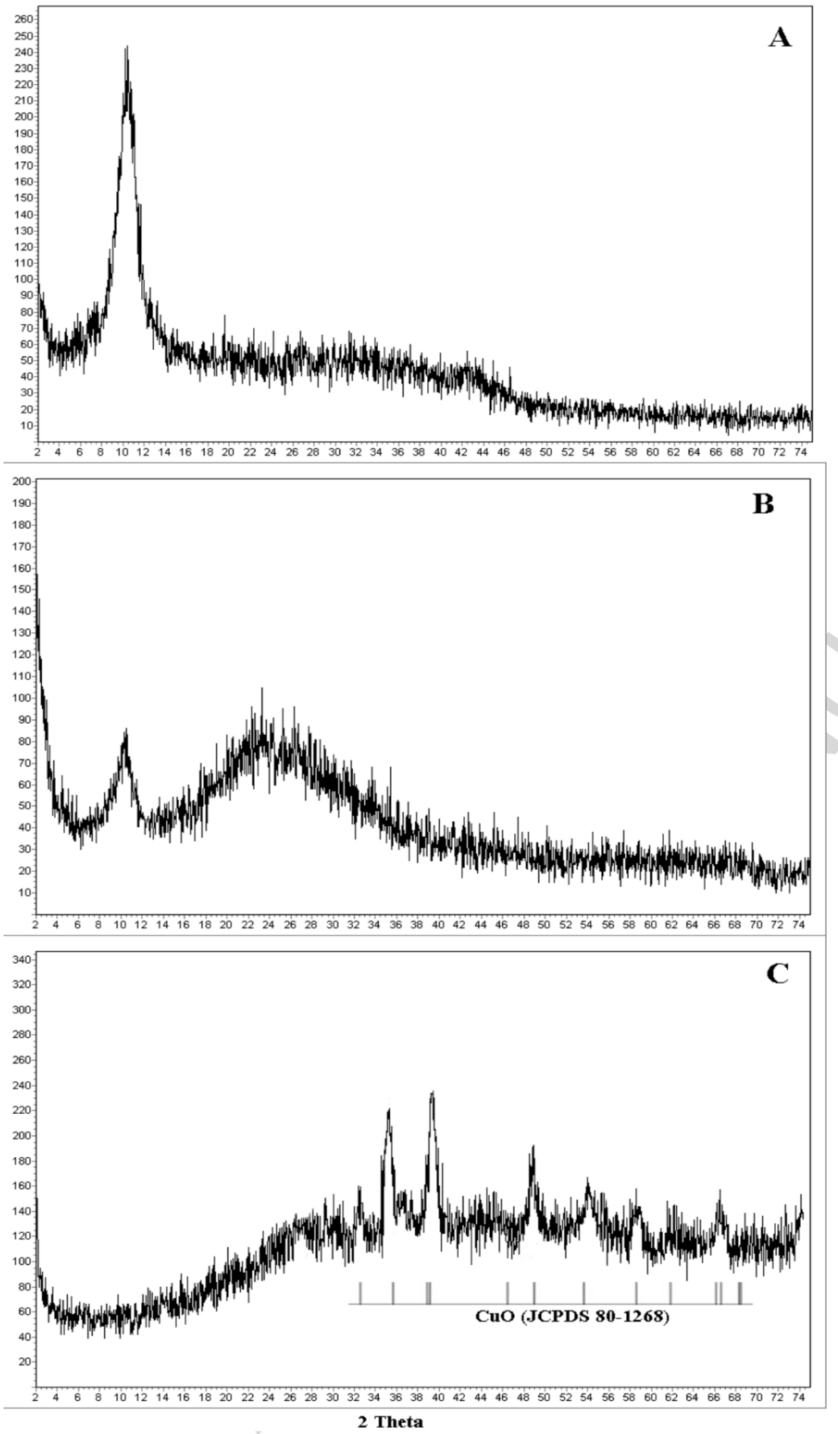

4.2 FTIR

The NFG (natural flake graphite powder), GO, and RGO functional groups were identified via FTIR analysis. The FTIR spectra of NFG, GO, and RGO powders are shown in Figure 25,26 and 27. The NFG spectrum displays an O-H broad peak at 3433.41 cm^{-1} due to intercalated water and a C = C at 1629.90 cm^{-1} attributed to graphitic domain skeletal vibrations. After oxidation of NFG, oxygen-containing groups such as functional hydroxyl, epoxy, and carboxylic groups were introduced, as shown in (Figure 26). Stretching vibration modes of C = O in carboxylic acid and carbonyl groups are responsible for the strong band at 1728.28 cm^{-1}. The skeletal vibrations of un-oxidized graphitic domains are responsible for the peak at 1624.12 cm^{-1}. C-O (epoxy) groups are represented by the band at 1057.03 cm^{-1}, whereas C-OH stretching vibrations are represented by the band at 1224.84 cm^{-1} and O-H stretching vibrations are represented by the band at 3433.41 cm^{-1}

Figure 25 FTIR spectrum of natural flake graphite powder

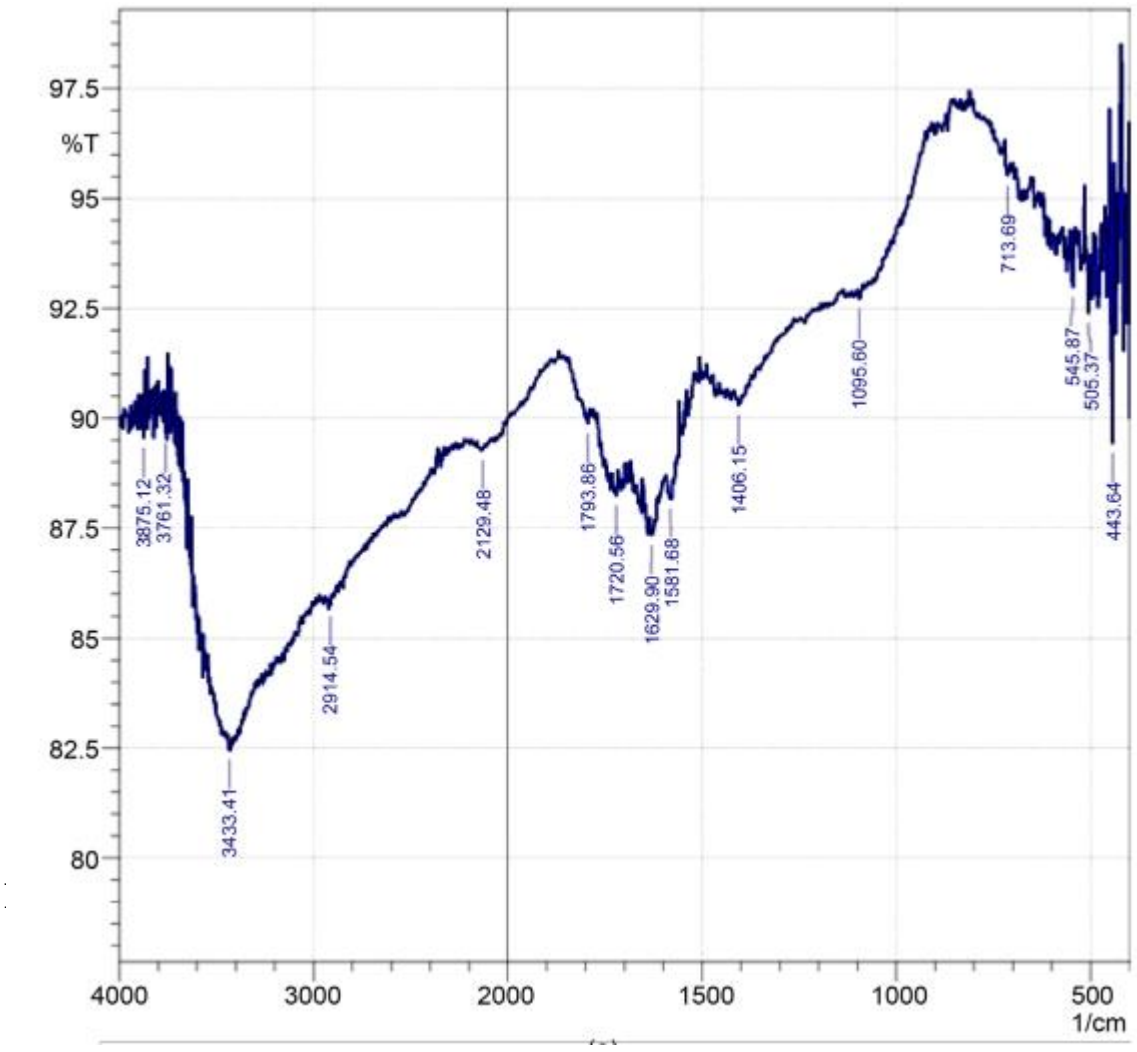

The bands associated with the oxygen-containing group were drastically reduced after the reduction process with N_2H_4. The broad band narrowed, and the carboxyl C = O peak at 1728.28 cm^{-1} vanished completely. C = N vibration is represented by the sharp peak at 1400.37 cm^{-1}, while C = C vibration is represented by the sharp peak at 1637.62 cm^{-1}. The hydrazine N_2H_4 utilized to reduce GO to RGO provided amine group functionality. [35]

Figure 26 FTIR spectrum of GO powder

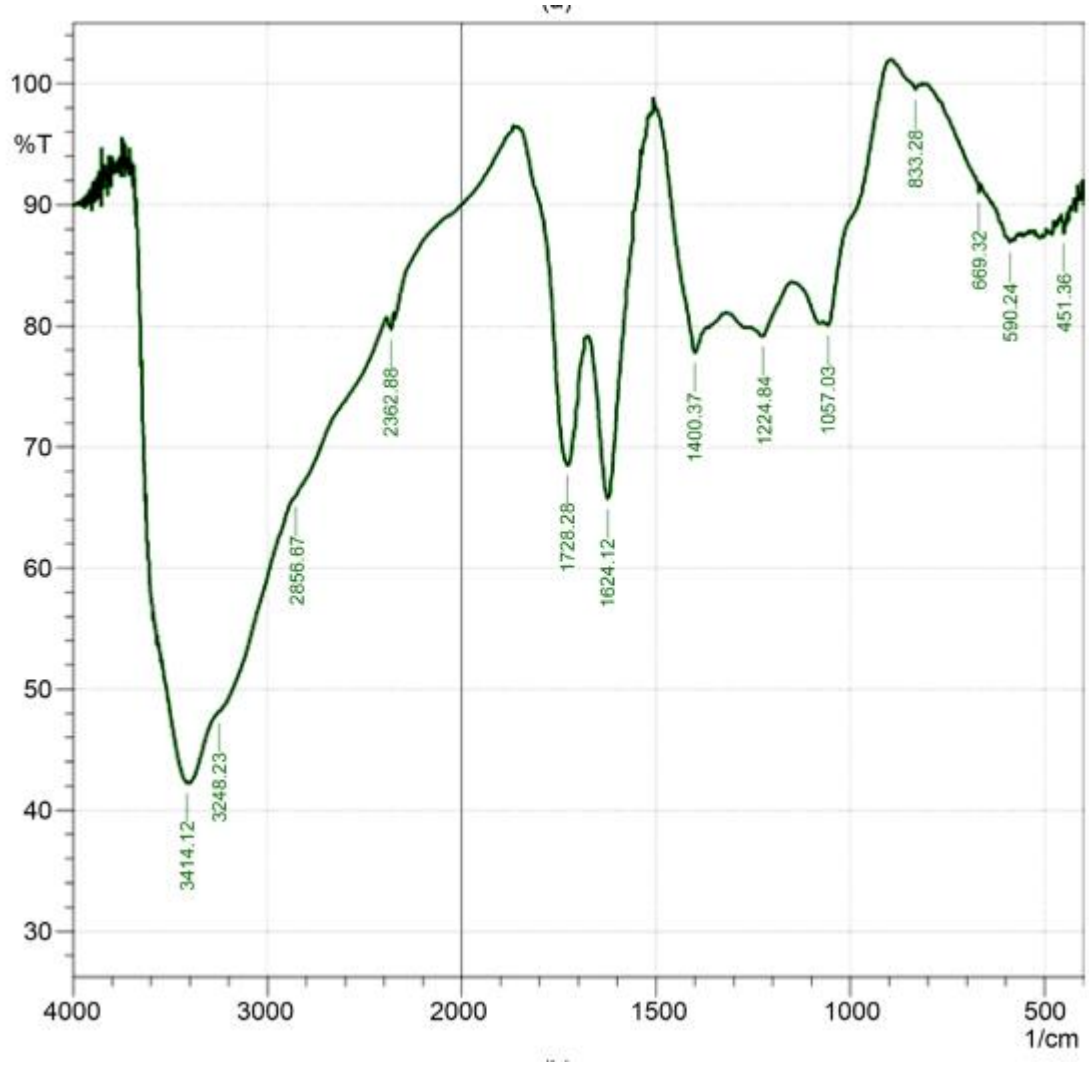

Figure 28 shows FTIR analysis of the chemical structures of rGO and rGO-CuO NPs to explore the shifting of chemical functional groups. The FT-IR spectra of rGO revealed many functional group peaks, including those centered at 3430 cm^{-1} (O-H), 1651 cm^{-1} (C=C), and 1282 cm^{-1} (C–O). Furthermore, the unique peaks centered at 2920 cm^{-1} and 1421 cm^{-1} were linked to C–H bonds in $–CH_3$ and $–CH_2$, as well as C–H in-plane bending vibrations (Figure 28). [36]

Most noteworthy, functional groups revealed several differences between rGO and rGO-CuO NPs. At stretching vibration 3440 cm^{-1} and 3350 cm^{-1}, the distinctive peak centered at 3430 cm^{-1} was separated into two distinct peaks, both ascribed to O–H. C=adsorption C's peak of 1651 cm^{-1} was also lowered to 1620 cm^{-1}. In contrast, several peaks centered at 2920 cm^{-1}, 1421 cm^{-1}, and1282 cm^{-1} vanished, while others centered at 1380 cm^{-1}, 981 cm^{-1}, 916 cm^{-1}, and 842 cm^{-1} reappeared. These findings suggested that CuO NPs had been successfully adsorbed on the surface of rGO nanosheets. [2]

Figure 27 FTIR spectrum of RGO powder.

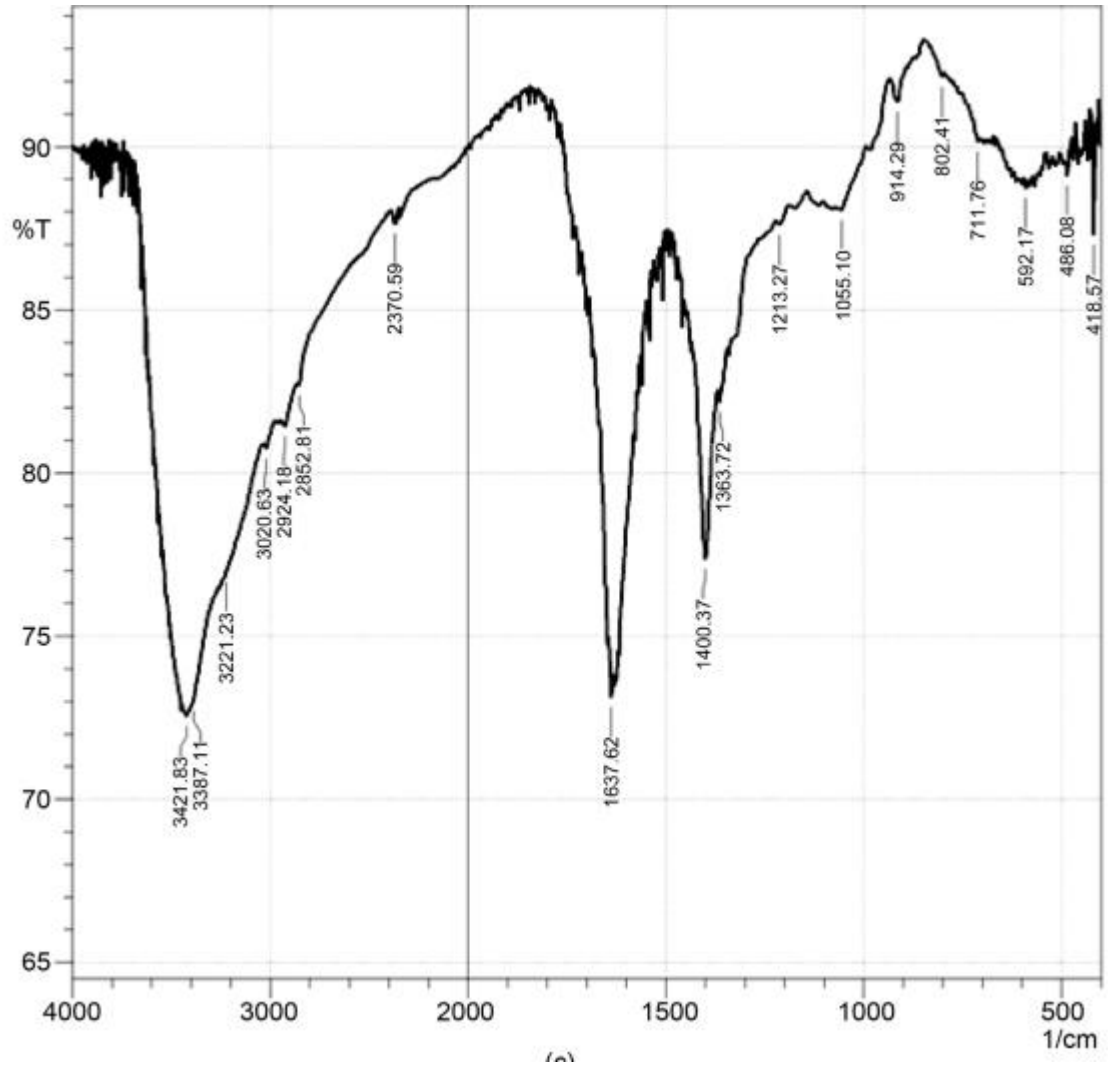

Figure 28 FT-IR spectra of rGO and rGO-CuO NPs, as indicated.

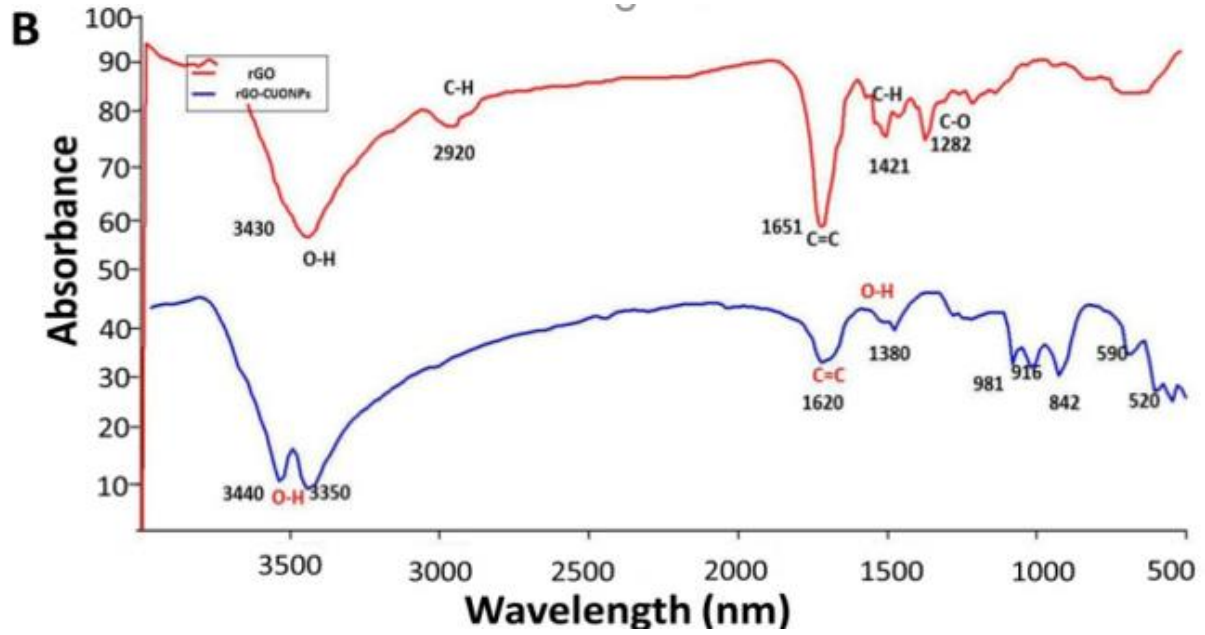

4.3 EDS/EDX

(Figure 29) depicts the elemental mapping of the rGO-CuO nanocomposite using EDAX, as well as the derived findings. It specifies that the rGO-CuO sample's elemental mapping contains 39 percent Cu, 49 percent O, and 12 percent C. This validates the presence of rGO in the rGO-CuO sample, indicating that the CuO particles are dispersed uniformly across the graphene layers. Furthermore, the amount of C is very low (and thus could not be detected in the XRD), indicating a decrease in the C dispersion in the nanocomposite. It's partly related to the graphene quenching of the GO. The rGO-CuO nanocomposites were successfully produced without any impurities, according to the overall examination of EDAX, and EDS. [37]

Figure 29(a) EDAX analysis of the produced rGO-CuO composite and (b–e) EDS mappin

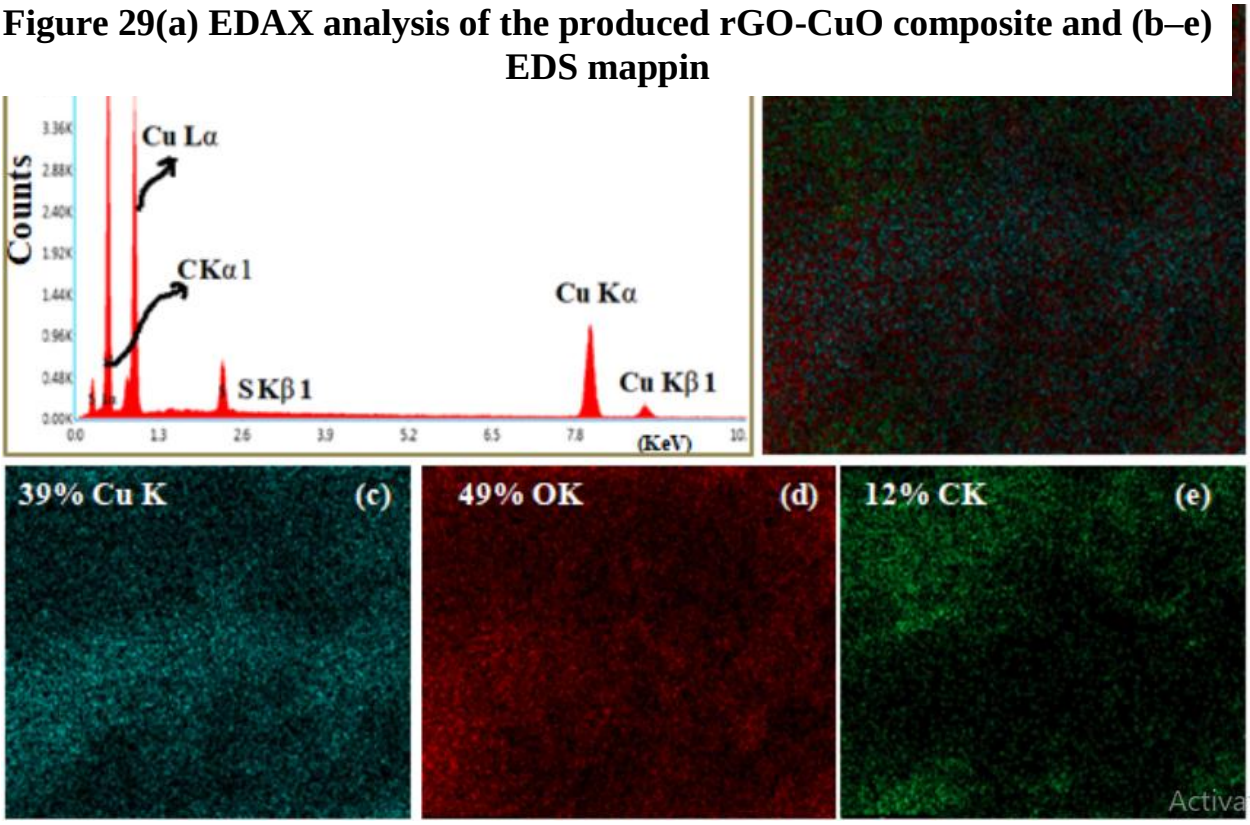

4.4TEM

The synthesis of CuO nanoparticle-decorated rGO is shown in Fig. 30a, which is a low magnification TEM image of the products. The high magnification TEM image (Fig. 30b) also demonstrates that the nanoparticle is flower-shaped and made up of smaller nanoparticles, implying the development of CuONF/ rGO. Because of the presence of PQ11, which has been employed as an effective stabilizing agent for rGO and metal nanoparticles in our earlier investigations, the dispersion of the resulting CuONF/rGO can be well-stable for several weeks without the observation of any floating or precipitate particles.[32]

Figure 30 CuONF/rGO nanocomposites TEM pictures

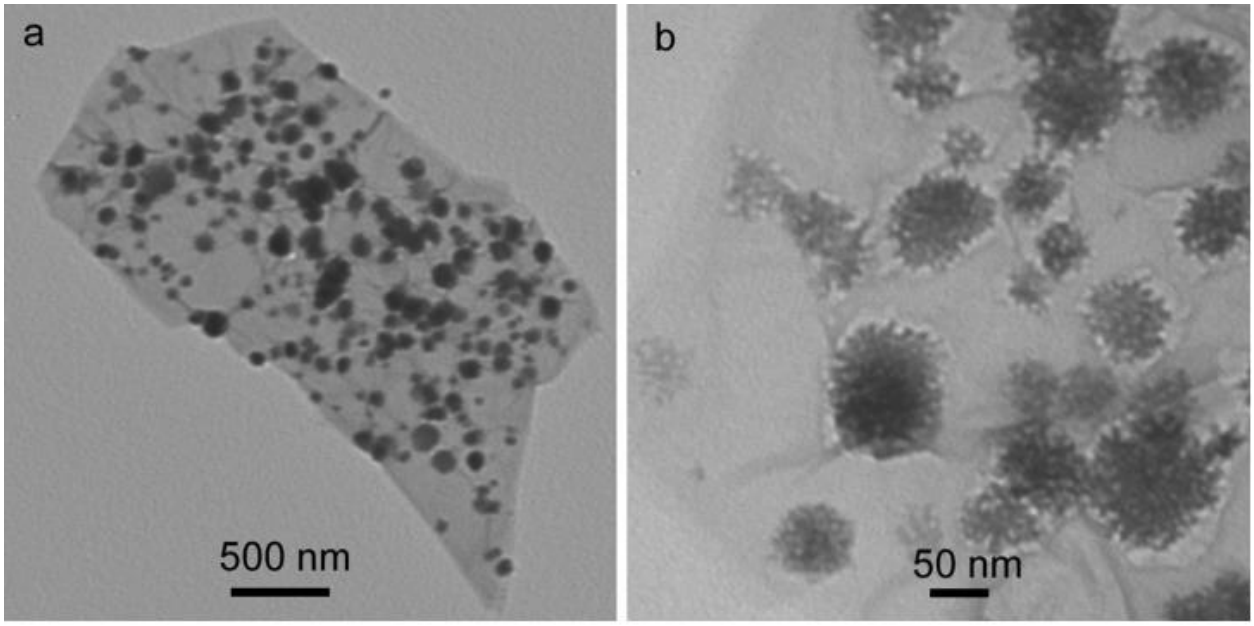

CHAPTER 5: RESULTS AND DISCUSSION

5.1 CFU Count

As shown in Figure 31, rGO/Cu(s) mediated considerable bactericidal action for each type of bacterial strain in an agar plate culture experiment. In comparison to the control (untreated) and GO-treated samples, the rGO–Cu(s) samples had the smallest number of colonies. [38]

Figure 31 Images of the antibacterial assay's agar plates

5.2 Inhibition Zone

GO and the rGO/CuO nanomaterial were tested for antibacterial activity against E. cherichia coli bacteria using the Agar well diffusion method and levofloxacin as a bacterium standard. The antimicrobial activity was identified by forming a zone of inhibition. The antibacterial activity of GO and the produced rGO/CuO nanocomposite were compared using a microdilution and live/dead technique. Figures 3 and 4 show representative pictures of antimicrobial petri plates, with "S1" representing "GO" and "S2" representing the rGO/ CuO nanocomposite. The suppression of bacterial colonies was visible after 24 hours of incubation. The incubation also revealed obvious inhibitory zones in the agar plate. The GO and rGO/CuO nanocomposite concentrations were both 50 µg. Antibacterial activity of E. coli gram-negative bacteria is shown in Figure . [39]

The antimicrobial properties of the synthesized GO and rGO/CuO nanocomposite against bacteria, E. coli, are shown in Table 3. The rGO/CuO nanocomposite created a somewhat better inhibitory zone of 13 mm on E. coli bacteria than the GO nanocomposite (11 mm inhibition zone). [39]

Figure 32 Image of anti-bacterial activity with: E. coli

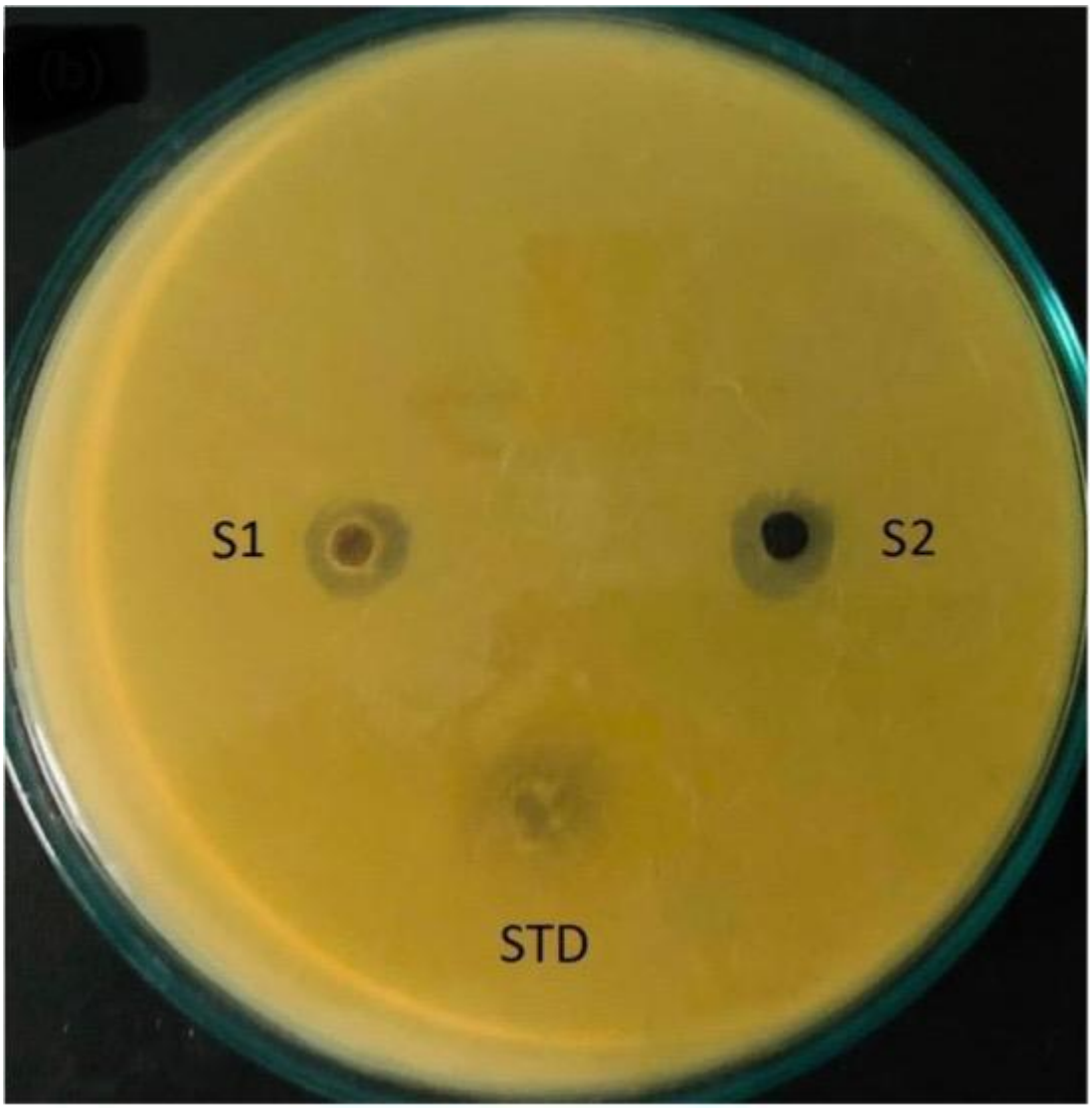

Table 3 Antimicrobial activity of GO and the rGO/CuO nanocomposite against Escherichia coli

Bacteria	S1 (zone in mm)	S2 (zone in mm)
Escherichia coli	11	13

5.3 Antibacterial mechanism

Two mechanisms were proposed for the antibacterial activity of the nanocomposite films: membrane perturbation and oxidative stress.

To investigate the impact of membrane perturbation on bacterial cell inactivation, SEM images of the attached bacterial cells on the films were captured

Figure 33 Representation SEM images of E coli on (a) rGO, (b) rGO-CuO

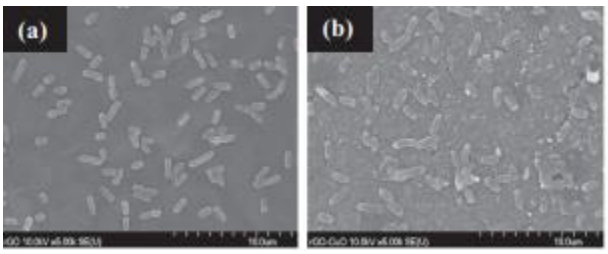

The morphology of the attached bacterial cells on the rGO film shows no cell membrane damage. The attached bacterial cells on rGO-CuO. This could have resulted from the impact of the nanorods on the bacterial cells. Regardless of the formation of nanorods, the increased surface area of the rGO-CuO composite films enhanced their antibacterial activity conclusively.

Another proposed mode of antibacterial action is oxidative stress, where cell inactivation is induced by the oxidation of vital cellular components or structures. Herein, chemical probes were used to access both indirect reactive oxygen species (ROS), mediated oxidative stress and ROS dependent oxidative stress. Glutathione (GSH) oxidation of measured to mimic intracellular oxidative stress [40]. GSH is a tripeptide molecule with a thiol group attached to it present in most gram-negative bacteria [42]. This intracellular compound can safeguard cellular components against oxidative stress. When the thiol group is oxidized to a disulfide bond, glutathione disulfide is formed. By measuring the number of GSH thiol groups lost during the generation of oxidative stress, Ellman's assay can be used to monitor the production of oxidative stress. In this study, the loss of oxidation was assessed during the incubation of the pristine rGO and rGO-CuO (rGO-CuO: 71.5%) nanocomposite films. As shown in

Figure 34 Glutathione oxidation by the nanocomposite films

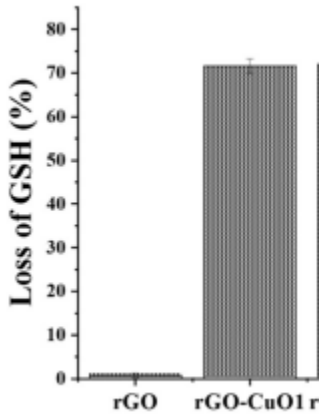

This result confirms that rGO-CuO nanocomposite films could initiate oxidative stress unlike the pristine rGO because of the incorporation of CuO into the composite.

Two pathways could be responsible for the oxidation of GHS: ROS generation and direct electron transfer. But we don't perform the ROS generation experiment.

The electron transfer property of CuO in the nanocomposite acts as a conductive bridge across the isolating lipid bilayer of the bacterial cells, thereby releasing cellular energy into the external environment [41]. Since bacterial cells can maintain a negative resting potential between -200 mV and -20 mV, [44]it is expected that they can readily lose electrons when their membrane potential is negative. Consequently, bacterial cell contact with Cu can form a circuit for electron transfer. This phenomenon is consistent with the findings of Li et al. [45], who linked charge transfer to the antimicrobial property of large-area monolayer graphene films. In their research, monolayer graphene was applied to the conductor Cu, the semiconducting Ge, and the insulator SiO_2. According to the findings of their study, the antimicrobial property of monolayer graphene on a conductor is greater than that of graphene on a semiconductor, whereas graphene on an insulator could not inhibit bacterial growth. This was explained by graphene's ability to function as a semiconductor, which allows it to transfer electrons to substrates. Cu, a conductor, was able to rapidly transfer electrons from the graphene film, resulting in the death of bacteria. Although Ge, a semiconductor, can transfer electrons, its ability is weaker than that of a conductor. SiO_2, an insulator, was incapable of any electron transfer; therefore, no bacterial inactivation was observed on graphene film on SiO_2.

The loss of electrons from the bacterial cell wall would automatically interrupt the electron transport chain in membrane respiration, resulting in the deactivation of the cell [46].

CHAPTER 6: CONCLUSION

From our examination we can conclude that

1 Due to introduction of CuO onto the RGO sheet the bacterial resistance has increased.
2 The inhibition zone has also increased due to CuO nanoflower structure.
3 Oxidative stress is the main reason for the increasement of resistance against bacteria.
4 Membrane perturbation also be reason for this.

References

[1] K. S. Novoselov *et al.*, "Electric field in atomically thin carbon films," *Science (80-.).*, vol. 306, no. 5696, pp. 666–669, 2004, doi: 10.1126/science.1102896.

[2] B. C. Brodie, "On tha Atomic Weight of Graphite," *Philos. Trans. R. Soc. B Biol. Sci.*, vol. 303, no. 1113, pp. 1–62, 1983, [Online]. Available: http://rstb.royalsocietypublishing.org/cgi/doi/10.1098/rstb.1983.0080

[3] H. P. Boehm, A. Clauss, G. O. Fischer, and U. Hofmann, "Das Adsorptionsverhalten sehr dünner Kohlenstoff-Folien," *ZAAC - J. Inorg. Gen. Chem.*, vol. 316, no. 3–4, pp. 119–127, 1962, doi: 10.1002/zaac.19623160303.

[4] S. Morichi, Y. Okahiro, Y. Komoda, H. Inagaki, and H. Itami, "Examination on the vertical normal strain observed at the grounds surface during earthquakes," *Doboku Gakkai Ronbunshuu A*, vol. 64, no. 2, pp. 452–457, 2008, doi: 10.2208/jsceja.64.452.

[5] T. W. Ebbesen and H. Hiura, "Graphene in 3-dimensions : Towards graphite origami," *Adv. Mater.*, vol. 7, no. 6, pp. 582–586, 1995, doi: 10.1002/adma.19950070618.

[6] A. K. Geim, "Graphene prehistory," *Phys. Scr.*, vol. 014003, no. T146, 2012, doi: 10.1088/0031-8949/2012/T146/014003.

[7] P. A. Denis and F. Iribarne, "Comparative study of defect reactivity in graphene," *J. Phys. Chem. C*, vol. 117, no. 37, pp. 19048–19055, 2013, doi: 10.1021/jp4061945.

[8] G. Diankov, M. Neumann, and D. Goldhaber-Gordon, "Extreme monolayer-selectivity of hydrogen-plasma reactions with graphene," *ACS Nano*, vol. 7, no. 2, pp. 1324–1332, 2013, doi: 10.1021/nn304903m.

[9] Y. Yamada *et al.*, "Subnanometer vacancy defects introduced on graphene by oxygen gas," *J. Am. Chem. Soc.*, vol. 136, no. 6, pp. 2232–2235, 2014, doi: 10.1021/ja4117268.

[10] C. Lee, X. Wei, J. W. Kysar, and J. Hone, "Measurement of the elastic properties and intrinsic strength of monolayer graphene," *Science (80-.).*, vol. 321, no. 5887, pp. 385–388, 2008, doi:

10.1126/science.1157996.

[11] P. Zhang *et al.*, “Fracture toughness of graphene,” *Nat. Commun.*, vol. 5, pp. 1–7, 2014, doi: 10.1038/ncomms4782.

[12] X. Wang, L. Zhi, and K. Mu, “透明電極1.Pdf,” *Nano Lett.*, vol. 8, N0. 1, pp. 323–327, 2008.

[13] S. Graphene *et al.*, “Organic Light-Emitting Diodes on,” vol. 4, no. 1, pp. 43–48, 2010.

[14] A. Safari, P. Hosseiniun, I. Rahbari, and M. R. Kalhor, “Graphene Based Electronic Device,” *Int. J. Electr. Comput. Energ. Electron. Commun. Eng.*, vol. 8, no. 8, pp. 1198–1203, 2014.

[15] C. H. Lui, L. Liu, K. F. Mak, G. W. Flynn, and T. F. Heinz, “Ultraflat graphene,” *Nature*, vol. 462, no. 7271, pp. 339–341, 2009, doi: 10.1038/nature08569.

[16] S. Pei and H. M. Cheng, “The reduction of graphene oxide,” *Carbon N. Y.*, vol. 50, no. 9, pp. 3210–3228, 2012, doi: 10.1016/j.carbon.2011.11.010.

[17] D. M. SHAPIRO, J. EIGNER, and G. R. GREENBERG, “Inability of Thymine-Dependent Mutants of Bacteriophage T4 To Induce,” *Proc. Natl. Acad. Sci. United States*, vol. 53, no. 22, pp. 874–881, 1965, doi: 10.1073/pnas.53.4.874.

[18] J. I. Paredes, S. Villar-Rodil, A. Martínez-Alonso, and J. M. D. Tascón, “Graphene oxide dispersions in organic solvents,” *Langmuir*, vol. 24, no. 19, pp. 10560–10564, 2008, doi: 10.1021/la801744a.

[19] J. Kotakoski, “Atomic and electronic structure of graphene,” *Graphene Prop. Prep. Charact. Appl. Second Ed.*, pp. 15–26, 2021, doi: 10.1016/B978-0-08-102848-3.00003-7.

[20] J. I. Paredes, S. Villar-Rodil, P. Solís-Fernández, A. Martínez-Alonso, and J. M. D. Tascón, “Atomic force and scanning tunneling microscopy imaging of graphene nanosheets derived from graphite oxide,” *Langmuir*, vol. 25, no. 10, pp. 5957–5968, 2009, doi: 10.1021/la804216z.

[21] H. He, J. Klinowski, M. Forster, and A. Lerf, “A new structural model for graphite oxide,” *Chem. Phys. Lett.*, vol. 287, no. 1–2, pp. 53–56, 1998, doi: 10.1016/S0009-2614(98)00144-4.

[22] A. Lerf, H. He, M. Forster, and J. Klinowski, “Structure of graphite oxide revisited,” *J. Phys. Chem. B*, vol. 102, no. 23, pp. 4477–4482, 1998, doi: 10.1021/jp9731821.

[23] D. Pandey, R. Reifenberger, and R. Piner, “Scanning probe microscopy study of exfoliated oxidized graphene sheets,” *Surf. Sci.*, vol. 602, no. 9, pp. 1607–1613, 2008, doi:

10.1016/j.susc.2008.02.025.

[24] A. B. Kaiser, “Electronic transport properties of conducting polymers and carbon nanotubes,” *Reports Prog. Phys.*, vol. 64, no. 1, pp. 1–49, 2001, doi: 10.1088/0034-4885/64/1/201.

[25] Y. Kopelevich and P. Esquinazi, “Graph ene physics in graphite,” *Adv. Mater.*, vol. 19, no. 24, pp. 4559–4563, 2007, doi: 10.1002/adma.200702051.

[26] C. Gómez-Navarro, M. Burghard, and K. Kern, “Elastic properties of chemically derived single graphene sheets,” *Nano Lett.*, vol. 8, no. 7, pp. 2045–2049, 2008, doi: 10.1021/nl801384y.

[27] A. Incze, A. Pasturel, and P. Peyla, “Mechanical properties of graphite oxides: Ab initio simulations and continuum theory,” *Phys. Rev. B - Condens. Matter Mater. Phys.*, vol. 70, no. 21, pp. 1–4, 2004, doi: 10.1103/PhysRevB.70.212103.

[28] S. L. Percival and D. W. Williams, *Escherichia coli*, Second Edi. Elsevier, 2013. doi: 10.1016/B978-0-12-415846-7.00006-8.

[29] P. Rajapaksha *et al.*, “Antibacterial Properties of Graphene Oxide-Copper Oxide Nanoparticle Nanocomposites,” *ACS Appl. Bio Mater.*, vol. 2, no. 12, pp. 5687–5696, 2019, doi: 10.1021/acsabm.9b00754.

[30] H. S. Bhargav, S. D. Shastri, S. P. Poornav, K. M. Darshan, and M. M. Nayak, “Measurement of the Zone of Inhibition of an Antibiotic,” *Proc. - 6th Int. Adv. Comput. Conf. IACC 2016*, pp. 409–414, 2016, doi: 10.1109/IACC.2016.82.

[31] W. Shao, X. Liu, H. Min, G. Dong, Q. Feng, and S. Zuo, “Preparation, characterization, and antibacterial activity of silver nanoparticle-decorated graphene oxide nanocomposite,” *ACS Appl. Mater. Interfaces*, vol. 7, no. 12, pp. 6966–6973, 2015, doi: 10.1021/acsami.5b00937.

[32] S. Liu, J. Tian, L. Wang, Y. Luo, and X. Sun, “One-pot synthesis of CuO nanoflower-decorated reduced graphene oxide and its application to photocatalytic degradation of dyes,” *Catal. Sci. Technol.*, vol. 2, no. 2, pp. 339–344, 2012, doi: 10.1039/c1cy00374g.

[33] A. B. Alayande, M. Obaid, and I. S. Kim, “Antimicrobial mechanism of reduced graphene oxide-copper oxide (rGO-CuO) nanocomposite films: The case of Pseudomonas aeruginosa PAO1,” *Mater. Sci. Eng. C*, vol. 109, no. December 2019, p. 110596, 2020, doi: 10.1016/j.msec.2019.110596.

[34] S. Pourbeyram, J. Abdollahpour, and M. Soltanpour, “Green synthesis of copper oxide nanoparticles decorated reduced graphene oxide for high sensitive detection of glucose,” *Mater. Sci. Eng. C*, vol. 94, pp. 850–857, 2019, doi: 10.1016/j.msec.2018.10.034.

[35] M. S. Eluyemi *et al.*, “Synthesis and Characterization of Graphene Oxide and Reduced Graphene Oxide Thin Films Deposited by Spray Pyrolysis Method,” *Graphene*, vol. 05, no. 03, pp. 143–154, 2016, doi: 10.4236/graphene.2016.53012.

[36] S. E. El-Abeid, Y. Ahmed, J. A. Daròs, and M. A. Mohamed, “Reduced graphene oxide nanosheet-decorated copper oxide nanoparticles: A potent antifungal nanocomposite against fusarium root rot and wilt diseases of tomato and pepper plants,” *Nanomaterials*, vol. 10, no. 5, 2020, doi: 10.3390/nano10051001.

[37] S. Sagadevan *et al.*, “Enhanced photocatalytic activity of rgo-cuo nanocomposites for the degradation of organic pollutants,” *Catalysts*, vol. 11, no. 8, 2021, doi: 10.3390/catal11081008.

[38] M. Maiti, M. Sarkar, S. Maiti, and D. Liu, “Efficacy of shape-monitored reduced graphene oxide-copper nanohybrids: anti-bacterial attributes for food safety and dye degradation studies,” *New J. Chem.*, vol. 43, no. 2, pp. 662–674, 2019, doi: 10.1039/C8NJ04447C.

[39] S. Siddique *et al.*, “Photo-Catalytic and Anti-microbial Activities of rGO/CuO Nanocomposite,” *J. Inorg. Organomet. Polym. Mater.*, vol. 31, no. 3, pp. 1359–1372, 2021, doi: 10.1007/s10904-020-01760-x.

[40] R. C. Fahey, W. C. Brown, W. B. Adams, and M. B. Worsham, “Occurrence of glutathione in bacteria,” *J. Bacteriol.*, vol. 133, no. 3, pp. 1126–1129, 1978, doi: 10.1128/jb.133.3.1126-1129.1978.

[41] C. D. Vecitis, K. R. Zodrow, S. Kang, and M. Elimelech, “Electronic-structure-dependent bacterial cytotoxicity of single-walled carbon nanotubes,” *ACS Nano*, vol. 4, no. 9, pp. 5471–5479, 2010, doi: 10.1021/nn101558x.

[42] R. Fahey, W. Brown, W. Adams, M. Worsham, J. Bacteriol. 133 (1978) 1126–1129

[43] C.D. Vecitis, K.R. Zodrow, S. Kang, M. Elimelech, ACS Nano 4 (2010) 5471–5479.

[44] L. Cassimeris, G. Plopper, V.R. Lingappa, Lewin’s Cells, Jones & Bartlett Publishers, 2011.

[45] J. Li, G. Wang, H. Zhu, M. Zhang, X. Zheng, Z. Di, X. Liu, X. Wang, Sci. Rep. 4 (2014) 4359.

[46] P. Dimroth, G. Kaim, U. Matthey, J. Exp. Biol. 203 (2000) 51–59.

[47] Boehm H P, Setton R and Stumpp E 1986 Carbon 24 241

[48] Warner, J. (2013). Graphene. Oxford [etc.]: Academic Press. 9.

[49] T. Puiu, "Graphene sheets can repair themselves naturally", ZME Science, 2012.

[50] Becerril HA, Mao J, Liu Z, Stoltenberg RM, Bao Z, Chen Y. Evaluation of solution-processed reduced graphene oxide films as transparent conductors. ACS Nano 2008;2(3):463–70